2019

Ferroelectric tunnel junctions enhanced by a polar oxide barrier layer

Q. Yang, L. L. Tao, E. Y. Tsymbal, and V. Alexandrov

NANO LETTERS

Letter

Cite This: Nano Lett. 2019, 19, 7385−7393

pubs.acs.org/NanoLett

Ferroelectric Tunnel Junctions Enhanced by a Polar Oxide Barrier Layer

Qiong Yang,[*,†,‡] Lingling Tao,[§] Yuke Zhang,[‡] Ming Li,[§] Zhen Jiang,[†] Evgeny Y. Tsymbal,[*,§] and Vitaly Alexandrov[*,†]

[†]Department of Chemical and Biomolecular Engineering, University of Nebraska, Lincoln, Nebraska 68588, United States

[‡]School of Materials Science and Engineering, Xiangtan University, Xiangtan, Hunan 411105, China

[§]Department of Physics and Astronomy, University of Nebraska, Lincoln, Nebraska 68588, United States

Supporting Information

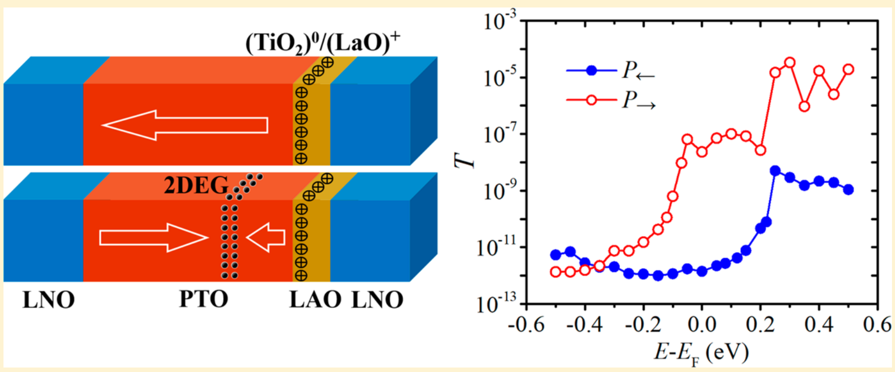

ABSTRACT: Ferroelectric tunnel junctions (FTJs) have recently aroused significant interest due to the interesting physics controlling their properties and potential application in nonvolatile memory devices. In this work, we propose a new concept to design high-performance FTJs based on ferroelectric/polar-oxide composite barriers. Using density functional theory calculations, we model electronic and transport properties of $LaNiO_3/PbTiO_3/LaAlO_3/LaNiO_3$ tunnel junctions and demonstrate that an ultrathin polar $LaAlO_3(001)$ layer strongly enhances their performance. We predict a tunneling electroresistance (TER) effect in these FTJs with an OFF/ON resistance ratio exceeding a factor of 10^4 and ON state resistance as low as about 1 k$\Omega\mu$m^2. Such an enhanced performance is driven by the ionic charge at the $PbTiO_3/LaAlO_3$ interface, which significantly increases transmission across the FTJ when the ferroelectric polarization of $PbTiO_3$ is pointing against the intrinsic electric field produced by this ionic charge. This is due to the formation of a two-dimensional (2D) electron or hole gas, depending on the $LaAlO_3$ termination being $(LaO)^+$ or $(AlO_2)^-$, respectively, which is formed to screen the polarization charge of the nonuniform polarization state. This 2D electron (hole) gas can be switched ON and OFF by the reversal of ferroelectric polarization, resulting in the giant TER effect. The proposed design suggests a new direction for creating FTJs with a stable and reversible ferroelectric polarization, a sizable TER effect, and a low-resistance-area product, as required for memory applications.

KEYWORDS: *Ferroelectric tunnel junctions, tunneling electroresistance effect, composite barrier, head-to-head domain wall, 2D electron gas, 2D hole gas*

Ferroelectric tunnel junctions (FTJs) have attracted a great deal of attention in recent years due to their potential for nonvolatile random-access memory applications.[1−7] A typical FTJ is constructed by sandwiching an ultrathin ferroelectric layer, which serves as an electron tunnel barrier, between two metal electrodes. Reversal of ferroelectric polarization leads to switching between two nonvolatile resistance states (low and high) of a FTJ, the phenomenon known as the tunneling electroresistance (TER) effect. A large TER effect is beneficial for practical applications. The structural and/or electronic asymmetry of the FTJ is known to play a decisive role in controlling the TER. It has been demonstrated that a sizable TER effect can be achieved by using dissimilar electrodes,[8−10] interface engineering,[11−15] applied bias,[16,17] or defect control.[18,19] Experimental studies have demonstrated that the OFF/ON resistance ratio in the FTJs with dissimilar electrodes can be as large as a few hundreds at room temperature.[4,20−22]

To further boost the TER effect, doped semiconductor/ferroelectric/metal heterostructures have been proposed and implemented.[23−29] In these FTJs, a Schottky barrier is controlled by ferroelectric polarization orientation through the tunable depletion and accumulation of majority carriers at the semiconductor/ferroelectric interface. The OFF/ON

Received: July 25, 2019
Revised: September 12, 2019
Published: September 13, 2019

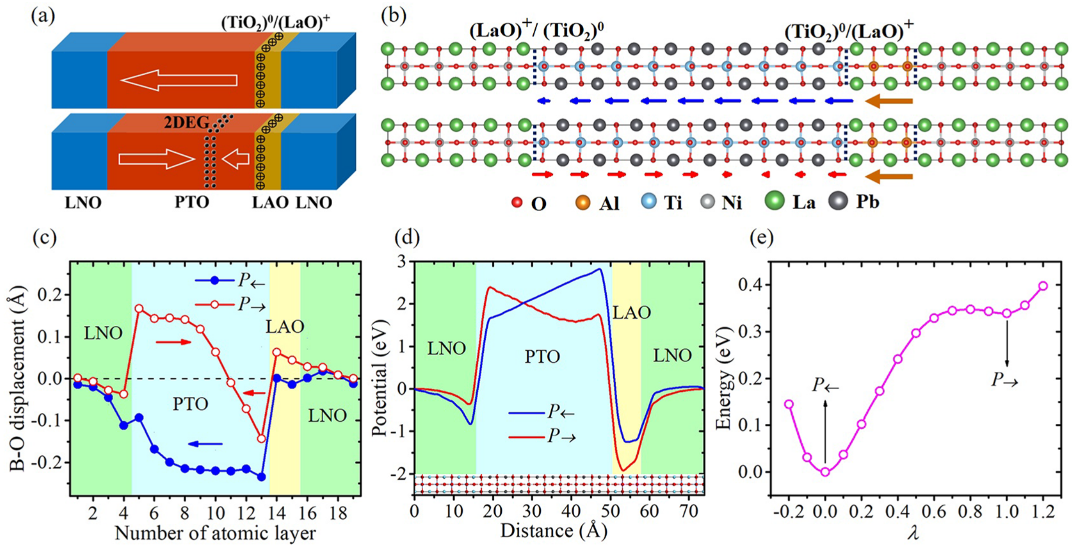

Figure 1. Structural and polarization properties of the PT-CB-FTJ. (a) The sketch of the $(TiO_2)^0/(LaO)^+$ terminated LNO/PTO/LAO/LNO tunnel junction for the $P_\leftarrow$ (top panel) and $P_\rightarrow$ (bottom panel) states. Symbols denote the positively charged interfacial $(LaO)^+$ atomic layer. The black small circles indicate the 2DEG formed at the head-to-head domain wall. (b) The atomic structures of the $P_\leftarrow$ (top panel) and $P_\rightarrow$ (bottom panel) states. The blue and red arrows below the atomic configurations indicate the local polarization of the PTO layer. The orange arrows denote the direction of the electric dipoles formed by the alternatively charged atomic layers of the LAO layer. (c) The B−O (B = Ti, Al, and Ni) polar displacements of each atomic layers. (d) The averaged electrostatic potential energy along the z-direction for the two polarization states. (e) The energy barrier for the polarization switching. Parameter λ scales the polarization state from $P_\leftarrow$ (λ = 0) to $P_\rightarrow$ (λ = 1).

resistance ratio of the doped semiconductor/ferroelectric/metal FTJs can be as large as 10^4 and even higher, suggesting that this type of FTJs is promising for nonvolatile memory applications. Unfortunately, due to a sizable Schottky barrier, these FTJs exhibit a very high-resistance-area (RA) product (typically exciding tens of M$\Omega\mu m^2$) that is prohibitive for the integration of FTJ devices into the modern complementary metal-oxide semiconductor (CMOS) electronics. Reducing the RA product by using a thinner ferroelectric barrier layer does not solve the problem due to a diminished OFF/ON resistance ratio as well as reduced polarization stability.

It has been proposed that composite ferroelectric/paraelectric barriers can be used to enhance the TER effect.[30,31] In such a composite barrier FTJ (CB-FTJ), the paraelectric layer acts as a switch changing the barrier height from a low to high value (or vice versa) when the ferroelectric polarization is reversed, resulting in an greater OFF/ON resistance ratio. Detailed first-principles studies of the $Pt/BaTiO_3/SrTiO_3/Pt$ FTJs[32] indicated that the composite $BaTiO_3/SrTiO_3$ barrier supports a switchable two-dimensional electron gas (2DEG) at its interface, resulting not only in a large TER value but also in a reduced RA product. The latter is due to the appearance of a 2DEG in the barrier region, which strongly reduces the ON-state resistance of the CB-FTJ. A switchable 2DEG at the interface between ferroelectric and nonpolar oxide layers was proposed previously,[33,34] but unfortunately has never been experimentally observed. In addition, the practical realization of CB-FTJs based on composite $BaTiO_3/SrTiO_3$ barrier layers[35] showed that although the OFF/ON resistance ratio was indeed very large (~10^3−10^4 at room temperature), the ON state RA product was too high (~50−200 M$\Omega\mu m^2$ for FTJs with a composite barrier thickness of about 4 nm) to be suitable for nonvolatile memories. This fact indicated that there was likely no 2DEG formed at the $BaTiO_3/SrTiO_3$ interface in these CB-FTJs, which could support the required low resistance of the FTJs in the ON state.

In contrast, there exists a large amount of evidence suggesting the existence of a 2DEG at the interface between polar and nonpolar oxide layers, such as $LaAlO_3/SrTiO_3$.[36,37] In these heterostructures, the interruption of the alternating sequence of positively and negatively charged ionic layers of the polar oxide leads to the electronic reconstruction at the interface.[38] Depending on the interface termination, a 2DEG or its counterpart, a two-dimensional hole gas (2DHG),[39] can emerge at the interface. It has been demonstrated that the 2DEG at the polar/nonpolar oxide interface can be tailored by gate voltage,[40] epitaxial strain,[41] mechanical loading,[42,43] and, more importantly for our studies, by ferroelectric polarization.[44−49] The latter fact indicates that using a polar oxide layer as a paraelectric component in a composite ferroelectric/paraelectric barrier in a CB-FTJ may be more promising than using its nonpolar counterpart. Such a ferroelectric/polar-oxide barrier is expected to support a switchable 2DEG or 2DHG in the CB-FTJ, resulting in a sizable TER effect and a low resistance of the ON state.

In this Letter, we propose $LaNiO_3/PbTiO_3/LaAlO_3/LaNiO_3$ oxide heterostructures as promising candidates to realize CB-FTJs with the required properties. Using first-principles density functional theory calculations, we predict that these junctions exhibit a switchable 2DEG or 2DHG, leading to a large TER effect and a low resistance in the ON state. In our proposed junctions, a composite barrier consists of a perovskite ferroelectric $PbTiO_3$ (PTO) layer and ultrathin polar insulating $LaAlO_3$ (LAO) layer. $LaNiO_3$ (LNO), a well-known paramagnetic metal,[50−52] serves as a perovskite oxide electrode.[14,53] We design two types of CB-FTJs, which are distinguished by ferroelectric/polar-oxide interface terminations of different polarities: positive $(TiO_2)^0/(LaO)^+$ and negative $(PbO)^0/(AlO_2)^-$. We find that, in the CB-FTJ with the positively charged $(TiO_2)^0/(LaO)^+$ termination (PT-CB-FTJ), switching ferroelectric polarization is associated with a transition between a uniformly polarized state and a head-to-

DOI: 10.1021/acs.nanolett.9b03056
Nano Lett. 2019, 19, 7385−7393

head polarization state with the domain wall parallel to the interface. While the uniformly polarized state has a high resistance, the head-to-head polarization state is accompanied by the formation of a 2DEG, strongly reducing the resistance of the CB-FTJ. The switchable 2DEG leads to a giant TER effect. In the CB-FTJ with the negatively charged $(PbO)^0/(AlO_2)^-$ termination (NT-CB-FTJ), switching ferroelectric polarization is associated with a transition between a uniformly polarized state and a state with strongly suppressed polarization at the $PbTiO_3/LaAlO_3$ interface. The latter is accompanied by the formation of a 2DHG at the ferroelectric/polar-oxide interface. The switchable 2DHG controls the TER effect and results in a reduced RA product for the ON state. These results suggest that FTJs with composite ferroelectric/polar-oxide barrier layers may serve as favorable candidates for nonvolatile memory applications.

Density functional theory (DFT) calculations are performed using the VASP code[54] to optimize the atomic structure of the CB-FTJs and study their electronic properties (see Supporting Information for details). The LNO/PTO/LAO/LNO tunnel junction with the $(TiO_2)^0/(LaO)^+$ termination at the ferroelectric/polar-oxide interface, as depicted in Figure 1a, is employed to model the PT-CB-FTJ. Figure 1b shows the optimized atomic structures of the $P_\leftarrow$ and $P_\rightarrow$ polarization states of the PT-CB-FTJ. Here, the periodic supercell is constructed by stacking 8.5 unit cell (u.c.) PTO, 2 u.c. LAO, and 8.5 u.c. LNO layers along the [001] direction. Both surfaces of PTO are terminated with the TiO_2 atomic layers in order to exclude the asymmetry induced by the different surficial terminations of the ferroelectric layer. The Ti−O polar displacements of each TiO_2 atomic layer are taken to represent the local polarization of the PTO layer as shown by the blue ($P_\leftarrow$) and red ($P_\rightarrow$) arrows under the atomic configurations in Figure 1b, whereas all of the B−O (B = Ti, Al, and Ni) displacements in the whole tunnel junction are plotted in Figure 1c.

We find that the observed polar displacements for both polarization states are largely controlled by the positively charged $(TiO_2)^0/(LaO)^+$ interface termination. For the $P_\leftarrow$ state, the whole PTO layer is uniformly polarized to the left with polarization near the LNO/PTO interface being slightly suppressed (the blue curve in Figure 1c). However, for the $P_\rightarrow$ state, the polarization of the PTO layer near the PTO/LAO interface is reversed against its bulk polarization (the red curve in Figure 1c). Such polarization reversal is caused by the positively charged $(TiO_2)^0/(LaO)^+$ termination of this interface, which electric field pins the polar displacements in the PTO layer near the interface away from it. Thus, in contrast to the uniformly polarized $P_\leftarrow$ state, the $P_\rightarrow$ state represents a head-to-head polarization configuration with the domain wall formed within the PTO layer close to the PTO/LAO interface. Such a local polarization pinning near the interface and the induced head-to-head domain wall have also been observed in the $Au/PbZr_{0.2}Ti_{0.8}O_3$/Nb-doped $SrTiO_3$ system, due to the positively charged surficial depletion layer of the Nb-doped $SrTiO_3$.[55]

The electrostatic potential energy profiles associated with the two polarization states in the $(TiO_2)^0/(LaO)^+$-terminated LNO/PTO/LAO/LNO tunnel junction are shown in Figure 1d. It is seen that the potential in the PTO layer increases almost linearly along the z-direction induced by the uniform polarization $P_\leftarrow$. When the polarization direction is poled to the right, the potential in the PTO layer decreases and then slightly increases. This increase is due to the presence of the head-to-head domain wall resulting in a V-shape potential profile in agreement with the previous report.[56] To evaluate the magnitude of the energy barrier for switching between the two polarization states, we carry out a series of static calculations along the pathway generated through a linear interpolation of the atomic coordinates $[z(\lambda) = (1 - \lambda)z\,(P_\leftarrow) + \lambda z\,(P_\rightarrow)]$ between the $P_\leftarrow$ ($\lambda = 0$) and $P_\rightarrow$ ($\lambda = 1$) states (Figure 1e). The obtained energy profile of the polarization switching indicates the bistable nature of the junction. We note that, although the potential well observed for the $P_\rightarrow$ state is relatively shallow, it can be deepened by increasing the PTO layer thickness. Therefore, it is suggested that the thickness of the PTO layer should be greater than 8 u.c. to achieve better stability of a head-to-head domain wall state in such an FTJ. Overall, our results predict a possibility of switching between the uniformly polarized state and the head-to-head polarization state for the LNO/PTO/LAO/LNO tunnel junction with a $(TiO_2)^0/(LaO)^+$ interfacial termination.

Next, we analyze the electronic structure properties of the PT-CB-FTJ. Figure 2 shows the layer-resolved local density of states (LDOS) projected onto the TiO_2 and AlO_2 atomic layers in the $(TiO_2)^0/(LaO)^+$-terminated LNO/PTO/LAO/LNO tunnel junction for the two polarization states. For the $P_\leftarrow$ state (Figure 2a), the conduction band minimum (CBM) and the valence band maximum (VBM) vary monotonically across the PTO and LAO layers in a similar way as the electrostatic potential in Figure 1d. For this polarization state, no 2DEG appears at the $(TiO_2)^0/(LaO)^+$-terminated PTO/LAO interface, in contrast to that normally observed at the STO/LAO interface with the same termination.[37] This is due

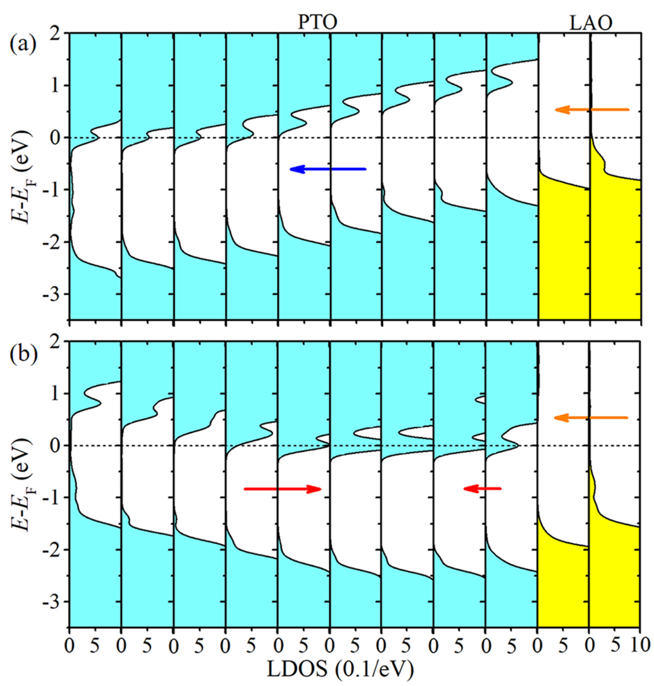

Figure 2. Local density of states of the PT-CB-FTJ. The layer-resolved local density of states (LDOS) projected onto the TiO_2 and AlO_2 atomic layers in the PTO and LAO regions for the $P_\leftarrow$ (a) and $P_\rightarrow$ (b) states of the $(TiO_2)^0/(LaO)^+$-terminated LNO/PTO/LAO/LNO tunnel junction. The horizontal dashed lines indicate the Fermi energy. The arrows denote the directions of polarization (in PTO) and the electric dipole (in LAO).

DOI: 10.1021/acs.nanolett.9b03056
Nano Lett. 2019, 19, 7385−7393

to the negative polarization charge at the right PTO surface, which largely compensates the positively charged $(LaO)^+$ layer, resulting in an essentially nonpolar PTO/LAO interface. We find, however, that the Fermi energy crosses the CBM of PTO closer to the LNO/PTO interface (about 4 u.c. from it, as seen from Figure 2a). This crossing is supported by the polar LNO/PBO interface, which $(LaO)^+/(TiO_2)^0$ termination reduces the electrostatic potential energy. In this case, the left 4 u.c. of the PTO layer serve as a continuation of the electrode rather than a tunnel barrier.

When the ferroelectric polarization is reversed to point to the LAO layer (Figure 2b), the variations of the CBM and VBM of PTO reveal the V-shape profile of the electrostatic potential energy (Figure 1d). This pushes the CBM below the Fermi energy, resulting in the electron accumulation and the formation of a 2DEG within about 6 u.c. layers of PTO adjacent to the PTO/LAO interface. The appearance of the 2DEG is driven by the head-to-head polarization configuration (Figure 1a, bottom panel), similar to that found for the head-to-head domain wall in a BTO thin film.[56] As seen from Figure 2b, the 2DEG is well separated from the left and right LNO electrodes by the potential barriers created by the PTO layer (on the left) and the LAO layer (on the right). The 2DEG is mainly formed by the Ti d_{xz} and d_{yz} orbitals as revealed by the orbital-resolved LDOS analyses in the Supporting Information.

Next, we explore the electron transport properties of the PT-CB-FTJ. The electron transmission is calculated within the general scattering formalism[57] implemented in Quantum ESPRESSO[58] (see Supporting Information for details). Figure 3a shows the calculated transmission, T, as a function of energy, E, for the $(TiO_2)^0/(LaO)^+$-terminated LNO/PTO/LAO/LNO tunnel junction. It is seen that, for the $P_\leftarrow$ state, the transmission changes slowly near the Fermi energy. Although the Fermi energy is crossing the CBM of PTO near the LNO/PTO interface, the density of states at the TiO_2 layers is rather small and does not affect the transmission dramatically when the energy is varied around the Fermi energy (Figure 2a). For the $P_\rightarrow$ state, however, the transmission increases substantially at about 0.1 eV below the Fermi energy, when the electron energy enters the 2DEG density (Figure 2b). This enhancement is due to resonant tunneling across the electronic states forming the 2DEG in the composite barrier. We find that transmission for the $P_\rightarrow$ state is 1.6×10^4 times higher compared to that of the $P_\leftarrow$ state at the Fermi energy. Due to the 2DEG, the resistance of the ON state is relatively low, such that the RA product is about 0.16 $M\Omega\mu m^2$. Thus, a giant TER effect and a low RA product are demonstrated for the $(TiO_2)^0/(LaO)^+$-terminated LNO/PTO/LAO/LNO tunnel junction due to the switchable 2DEG in the composite barrier.

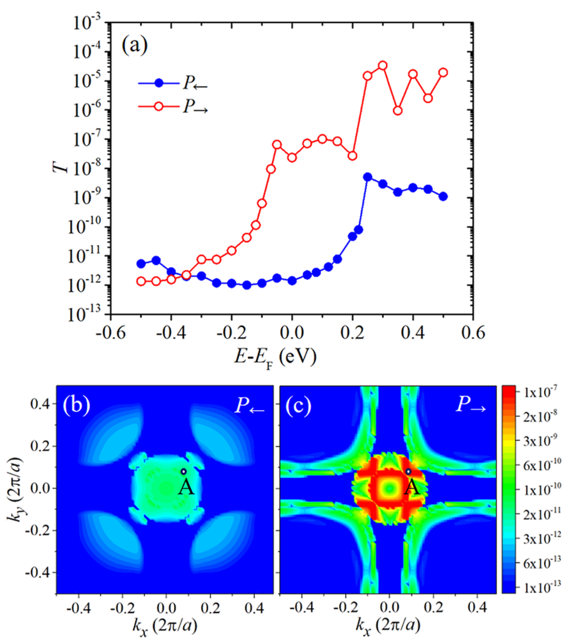

Figure 3. Transmission across the PT-CB-FTJ. (a) Transmission (T) per unit cell area across the $(TiO_2)^0/(LaO)^+$-terminated LNO/PTO/LAO/LNO tunnel junction as a function of incident electron energy, E, for $P_\leftarrow$ (blue solid symbols) and $P_\rightarrow$ (red open symbols) polarization states. (b, c) $\boldsymbol{k}_\parallel$-resolved transmission probabilities across the tunnel junction for $P_\leftarrow$ (b) and $P_\rightarrow$ (c) states. Point A denotes $\boldsymbol{k}_\parallel$ = (0.08, 0.08).

To provide further insights into the origin of the difference between electron transmission mechanisms for the two polarization states of the tunnel junction, we calculate the transmission probability as a function of transverse wave vector $\boldsymbol{k}_\parallel$ at the Fermi energy. The results are shown in Figures 3b and 3c. For the $P_\leftarrow$ state (Figure 3b), the $\boldsymbol{k}_\parallel$-resolved transmission probability is relatively small and is featured by the central circular region around the $\bar{\Gamma}$ point ($\boldsymbol{k}_\parallel = 0$) reflecting the respective Bloch states in bulk LNO at the Fermi energy (Figure S1g). Transmission within the four Fermi surface pockets around the corners the two-dimensional Brillouin zone (2DBZ), seen in Figure S1g, is strongly suppressed by the symmetry mismatch between the propagating electronic states in the LNO electrode and the evanescent states in PTO, similar to that found for the $La_{0.5}Sr_{0.5}MnO_3$/BTO/$La_{0.5}Sr_{0.5}MnO_3$ FTJ.[56] For the $P_\rightarrow$ state (Figure 3c), the $\boldsymbol{k}_\parallel$-resolved transmission map reveals a strong enhancement. In addition to the central circular region around the $\bar{\Gamma}$ point, there are four arcs around the corners of the 2DBZ and significantly enhanced transmission within the central region of the 2DBZ (indicated by the red contrast in Figure 3c). This enhanced transmission originates from tunneling across the electronic states forming the 2DEG. These states are localized in the transport direction and serve as resonant states for transmission. On the basis of the analysis of the $\boldsymbol{k}$-resolved LDOS projected onto the Ti atoms near the domain wall (Figure S1), we find that the resonant transmission originates from the hybridized Ti-d_{z^2} and Ti-$d_{xz,yz}$ states, supporting transmission of the propagating Bloch states of the d_{z^2} orbital character available in the LNO electrodes (see Supporting Information for details).

The effect of resonant transmission is also seen from the calculated partial charge density and scattering states at the Fermi energy (E_F) in the real space. The partial charge densities are obtained by integrating the LDOS from E_F, 0.1 eV to E_F and shown in Figures 4a and 4c, for the $P_\leftarrow$ and $P_\rightarrow$ states, respectively. The scattering states are obtained by calculating a squared wave function of the right-moving state at $\boldsymbol{k}_\parallel$ = (0.08, 0.08) (denoted by A in Figures 3b and 3c) and plotted in Figures 4b and 4d, for the $P_\leftarrow$ and $P_\rightarrow$ states, respectively. It is seen from Figure 4a that, for the $P_\leftarrow$ state, the partial charge density only exists in a few atomic layers near the LNO/PTO interface, corresponding to the layer resolved LDOS of PTO at the Fermi energy in Figure 2a. The electron state incident from the left LNO electrode decays very rapidly in the barrier region, as seen from Figure 4b. On the contrary,

DOI: 10.1021/acs.nanolett.9b03056
Nano Lett. 2019, 19, 7385−7393

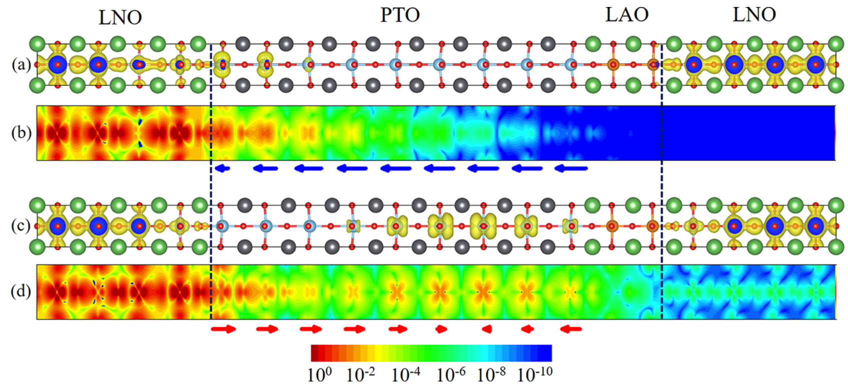

Figure 4. Partial charge densities and scattering states for the PT-CB-FTJ. (a, c) Partial charge densities and (b, d) real-space scattering states at the Fermi energy for the $(TiO_2)^0/(LaO)^+$-terminated LNO/PTO/LAO/LNO tunnel junction for the $P_{\leftarrow}$ (a, b) and $P_{\rightarrow}$ (c, d) states. The blue and red arrows indicate the local polarization of the PTO layer.

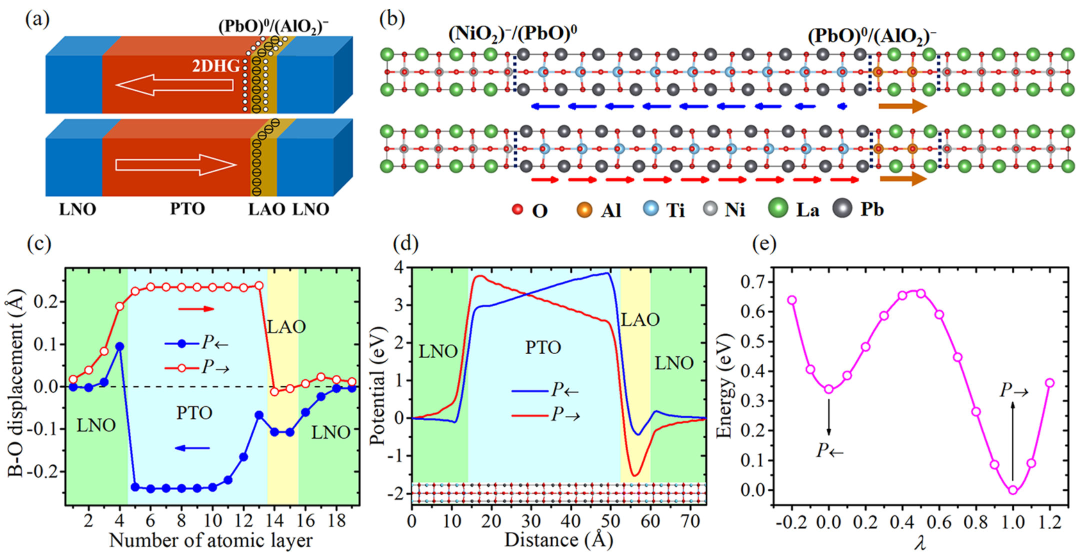

Figure 5. Structural and polarization properties of the NT-CB-FTJ. (a) The sketch of the $(PbO)^0/(AlO_2)^-$-terminated LNO/PTO/LAO/LNO tunnel junction for the $P_{\leftarrow}$ (top panel) and $P_{\rightarrow}$ (bottom panel) states. Symbols denote the negatively charged interfacial $(AlO_2)^-$ atomic layer. The white small circles indicate the 2DHG spreading across the PTO/LAO interface. (b) The atomic configurations of the $P_{\leftarrow}$ (top panel) and $P_{\rightarrow}$ (bottom panel) states. The blue and red arrows below the atomic configurations indicate the local polarization of the PTO layer. The orange arrows denote the direction of the electric dipoles formed by the alternatively charged atomic layers of the LAO layer. (c) The B−O (B = Ti, Al and Ni) polar displacements of each atomic layers. (d) The averaged electrostatic potential energy along the z-direction for the two polarization states. (e) The energy barrier for the polarization switching. Parameter λ scales the polarization state from $P_{\leftarrow}$ ($\lambda = 0$) to $P_{\rightarrow}$ ($\lambda = 1$).

for the $P_{\rightarrow}$ state, as seen from Figure 4c, there are abundant charge densities distributed within the domain wall region, corresponding to the LDOS profile in Figure 2b. This states support resonant transmission across the composed PTO/LAO barrier, as is evident from the enhanced density of the scattering states around the domain wall region in Figure 4d. The partial charge densities and the scattering states at the domain wall region are mainly composed of the Ti-$d_{xz,\,yz}$ and Ti-d_{z^2} orbitals.

In the following, we present the results for the LNO/PTO/LAO/LNO tunnel junction with the $(PbO)^0/(AlO_2)^-$ termination at the ferroelectric/polar-oxide interface (NT-CB-FTJ), which is schematically shown in Figure 5a. The employed supercell is constructed by stacking 9.5 u.c. PTO, 2 u.c. LAO, and 7.5 u.c. LNO layers, along the [001] direction (Figure 5b). Both surfaces of the PTO layer are terminated with the PbO atomic planes to keep the symmetry of surface terminations. Figure 5b shows the optimized atomic structures of the $P_{\leftarrow}$ and $P_{\rightarrow}$ states of NT-CB-FTJ. All of the B−O (B = Ti, Al, and Ni) polar displacements in the LNO/PTO/LAO/LNO tunnel junction are plotted in Figure 5c.

We find that the observed polar displacements for both polarization states are controlled by the negatively charged $(PbO)^0/(AlO_2)^-$ interface termination. For the $P_{\rightarrow}$ state, where the polarization points to the right, the polarization is largely uniform across the whole PTO layer (the red curve in Figure 5c). However, for the $P_{\leftarrow}$ state, where the polarization of the PTO layer points away from the PTO/LAO interface, the polarization near this interface is strongly suppressed (the blue curve in Figure 5c). This suppression of the interfacial polarization is due to the built-in electric field originating from the negatively charged $(AlO_2)^-$ surficial atomic layer of LAO and pointing opposite to the polarization. The electrostatic potential energy profile and the polarization switching barriers for the $(PbO)^0/(AlO_2)^-$-terminated LNO/PTO/LAO/LNO tunnel junction are calculated and shown in Figures 5d and 5e, respectively. The electrostatic potential energy (Figure 5d) varies linearly along the z-direction inside the PTO layer for

DOI: 10.1021/acs.nanolett.9b03056
Nano Lett. 2019, 19, 7385−7393

both polarization states, owing to the uniform polarization displacements. The calculated energy profiles for polarization switching (Figure 5e) reveal a deeper potential well for the $P_{\rightarrow}$ state ($\lambda = 1$) than for the $P_{\leftarrow}$ state ($\lambda = 0$), which is in contrast to the $(TiO_2)^0/(LaO)^+$-terminated LNO/PTO/LAO/LNO tunnel junction (Figure 1e).

Figure 6 shows the layer-resolved LDOS projected onto the TiO_2 and AlO_2 atomic layers in the $(PbO)^0/(AlO_2)^-$-terminated LNO/PTO/LAO/LNO tunnel junction. When the PTO layer is polarized to the left ($P_{\leftarrow}$ state), the Fermi energy crosses the VBM of LAO and PTO near the PTO/LAO interface (Figure 6a). This implies the appearance of a 2DHG at the ferroelectric/polar-oxide interface. The 2DHG originates from the polar discontinuity at the $(PbO)^0/(AlO_2)^-$-terminated interface. Both the negative ionic charge of the $(AlO_2)^-$ layer and the negative polarization charge at the PbO/AlO_2 interface increases the electrostatic potential energy, resulting in the Fermi energy crossing the VBM. This 2DHG is mainly composed of the O 2p orbitals, as revealed by the orbital-resolved LDOS analysis (Figure S4 in Supporting Information). When the polarization is pointing to the PTO/LAO interface ($P_{\rightarrow}$ state), the 2DHG at the PTO/LAO interface disappears. This is due to the polarization charge compensating the negatively charged $(AlO_2)^-$ interfacial atomic layer. We see therefore that the 2DHG in the $(PbO)^0/(AlO_2)^-$-terminated LNO/PTO/LAO/LNO tunnel junction can be controlled by polarization of the PTO layer.

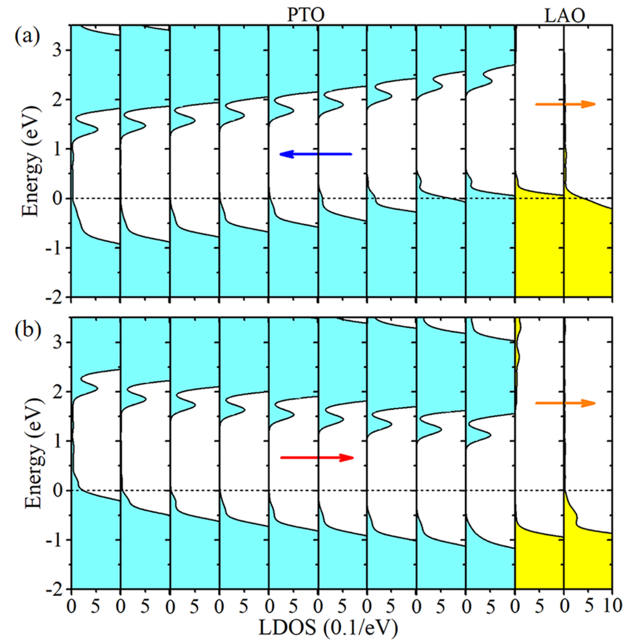

Figure 6. Local density of states of the NT-CB-FTJ. The layer-resolved local density of states (LDOS) projected onto the TiO_2 and AlO_2 atomic layers in the PTO and LAO regions for the $P_{\leftarrow}$ (a) and $P_{\rightarrow}$ (b) states of the $(PbO)^0/(AlO_2)^-$-terminated LNO/PTO/LAO/LNO tunnel junction. The horizontal dashed lines indicate the Fermi energy. The arrows denote the directions of polarization (in PTO) and the electric dipole (in LAO).

Next, we analyze the electron transmission, T, as a function of the electron energy, E, for the $(PbO)^0/(AlO_2)^-$-terminated LNO/PTO/LAO/LNO tunnel junction. As seen from Figure 7a, overall, the transmission decreases with increasing the energy. This trend is due to the energy moving deeper into the band gap (Figure 6), which enhances the decay rate of the evanescent states in the barrier region and thus reduces the transmission probability. The transmission differs by a few orders in magnitude for the two polarization states. The OFF/ON resistance ratio is estimated to be as large as 8.4×10^4. This is due to the significantly enhanced transmission probability for the $P_{\leftarrow}$ state, supporting the 2DHG. In fact, we find that the RA product for this polarization state (ON state) is as low as 1.4 k$\Omega\mu$m^2. Thus, a giant TER effect and a low RA product are demonstrated for the $(PbO)^0/(AlO_2)^-$-terminated LNO/PTO/LAO/LNO tunnel junction due to the switchable 2DHG in the composite barrier.

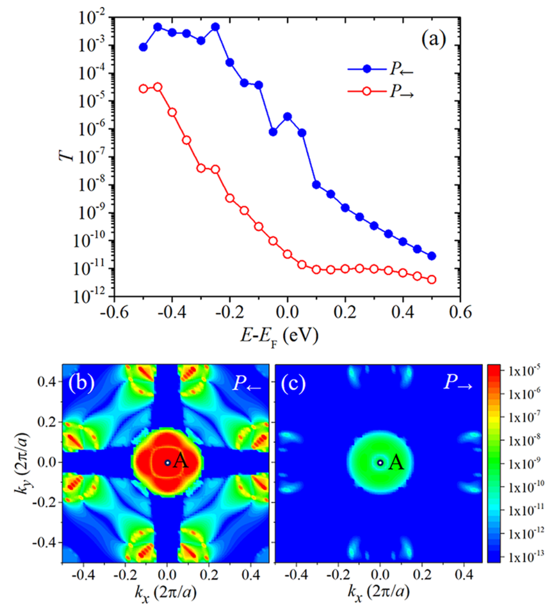

Figure 7. Transmission across the NT-CB-FTJ. (a) The transmission (T) per unit cell area across the $(PbO)^0/(AlO_2)^-$-terminated LNO/PTO/LAO/LNO tunnel junction as a function of E, for $P_{\leftarrow}$ (blue solid symbols) and $P_{\rightarrow}$ (red open symbols) states. (b and c) $\boldsymbol{k}_{\parallel}$-resolved transmission probabilities across the tunnel junction for $P_{\leftarrow}$ (b) and $P_{\rightarrow}$ (c) states.

The computed transmission probabilities as a function of transverse wave vector $\boldsymbol{k}_{\parallel}$ at the Fermi energy are plotted in Figures 7b and 7c for the two polarization states. In contrast to the $(TiO_2)^0/(LaO)^+$-terminated tunnel junction, the $\boldsymbol{k}_{\parallel}$-resolved transmission probability for the $P_{\leftarrow}$ state of $(PbO)^0/(AlO_2)^-$-terminated tunnel junction consists of one "hot" circle around the $\overline{\Gamma}$ point and four patterned fan-shaped areas around the corners of the 2DBZ. This hot circle originates from the enhanced transmission across the 2DEG and largely makes the transmission probability for the $P_{\leftarrow}$ state much higher than for the $P_{\rightarrow}$ state. On the basis of the analysis of the $\boldsymbol{k}_{\parallel}$-resolved LDOS projected onto the O atoms near the PTO/LAO interface (Figure S4), we find that the transmission of the $P_{\leftarrow}$ state is mostly determined by the O p_z states, which support transmission of the propagating states of the d_{z^2} orbital character available in the LNO electrodes (see Supporting Information for further discussion).

The effect of the 2DEG on transmission is also seen from the calculated partial hole density and scattering states at the Fermi energy (E_F) in the real space. The partial hole densities are obtained by integrating the LDOS from E_F to E_F + 0.1 eV and plotted in Figures 8a and 8c, for the $P_{\leftarrow}$ and $P_{\rightarrow}$ states, respectively. The corresponding right-moving scattering states

DOI: 10.1021/acs.nanolett.9b03056
Nano Lett. 2019, 19, 7385−7393

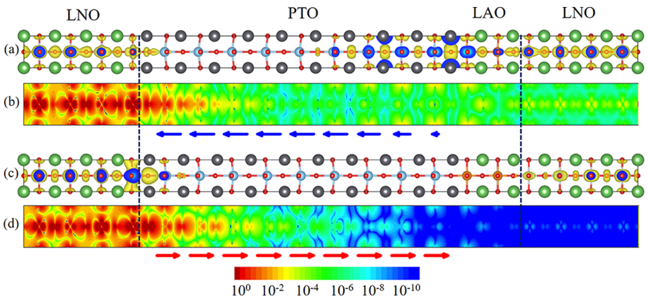

Figure 8. Partial charge densities and scattering states for the NT-CB-FTJ. (a,c) Partial charge densities and (b,d) real-space scattering states at the Fermi energy for the $(PbO)^0/(AlO_2)^-$-terminated LNO/PTO/LAO/LNO tunnel junction for the $P_\leftarrow$ (a,b) and $P_\rightarrow$ (c,d) states. The blue and red arrows indicate the local polarization of the PTO layer.

at $k_\parallel = (0, 0)$ (denoted by A in Figures 7b and 7c) at the Fermi energy are shown in Figures 8b and 8d for the $P_\leftarrow$ and $P_\rightarrow$ states, respectively. For the $P_\leftarrow$ state, large hole densities populate the PTO and LAO layers near the LNO/PTO interface (Figure 8a). These populated hole states strongly support the transmission so that the scattering state does not exhibit significant decay when propagating across the composite barrier (Figure 8b). The enhanced scattering amplitude is seen on the O-p_z orbitals pointing along the transport direction (Figure 8b). On the contrary, for the $P_\rightarrow$ state, only a few hole densities are seen near the LNO/PTO interface (Figure 8c), which leads to the rapid decay of the scattering states in the composite barrier (Figure 8d).

At the end, we would like note that Sanchez-Santolino et al.[59] have recently realized FTJs with a head-to-head domain wall parallel to the electrode/ferroelectric interface. Such a domain within the nm-thick barrier layer was stabilized by a confined 2DEG, which led to resonant tunneling across it and strongly enhanced conductance.[56,59,60] Unfortunately, in the experiment by Sanchez-Santolino et al.,[59] the domain wall was metastable; once it was destroyed by applying a sufficiently large electric field, it could not be restored. Our results indicate that using a composed ferroelectric/polar-oxide barrier could provide conditions for stabilizing a domain-wall-like state, supporting either 2DEG or 2DHG and resulting in a very high conductance. Although structural defects such as oxygen vacancies can be formed under experimental conditions, their role and influence on the results obtained for a defect-free FTJ can be the subject of a separate study.

In summary, we have proposed a new type of FTJs utilizing a composed ferroelectric/polar-oxide barrier layer. Using density functional theory and quantum transport calculations, we have explored $LaNiO_3/PbTiO_3/LaAlO_3/LaNiO_3$ tunnel junctions and demonstrated that an ultrathin polar $LaAlO_3$ (001) layer strongly enhances their performance. We considered different interface terminations of the composite $PbTiO_3/LaAlO_3$ barrier layer, i.e., $(TiO_2)^0/(LaO)^+$ and $(PbO)^0/(AlO_2)^-$, and in both cases found two reversible polarization states with one polarization state being nearly uniform and the other representing a strongly nonuniform polarization configuration. For the $(TiO_2)^0/(LaO)^+$-terminated tunnel junction, we obtained a head-to-head polarization state being stabilized by a 2DEG in the composite barrier region, whereas for the $(PbO)^0/(AlO_2)^-$-terminated tunnel junction, the strongly suppressed polarization at the $PbTiO_3/LaAlO_3$ interface was accompanied by a 2DHG. In both cases, the strongly enhanced transmission across the nonuniform polarization state led to a substantially reduced resistance with the resistance-area product as low as 1 k$\Omega\mu$m^2 and giant tunneling electroresistance with the OFF/ON resistance ratio exceeding 10^4. This performance of FTJs with ferroelectric/polar-oxide composite barriers is favorable for their application in nonvolatile memories. We hope therefore that our results will stimulate experimental efforts to explore such FTJs in practice and demonstrate the predicted properties.

■ ASSOCIATED CONTENT

Supporting Information

The Supporting Information is available free of charge on the ACS Publications website at DOI: 10.1021/acs.nanolett.9b03056.

Computational details for geometry optimization and electron transmission calculations, $k_\parallel$- and orbital-resolved local density of states (LDOS) for the on-state FTJ, and the effects of Hubbard U correction (PDF)

■ AUTHOR INFORMATION

Corresponding Authors

*E-mail: qyang@xtu.edu.cn.
*E-mail: tsymbal@unl.edu.
*E-mail: valexandrov2@unl.edu.

ORCID

Qiong Yang: 0000-0002-3235-1986
Zhen Jiang: 0000-0002-1175-5658
Evgeny Y. Tsymbal: 0000-0002-6728-5480
Vitaly Alexandrov: 0000-0003-2063-6914

Notes

The authors declare no competing financial interest.

■ ACKNOWLEDGMENTS

This work was supported by the National Science Foundation (NSF) through Nebraska MRSEC (DMR-1420645). Q.Y. thanks the China Scholarship Council (CSC) for financial support.

■ REFERENCES

(1) Tsymbal, E. Y.; Kohlstedt, H. Tunneling across a ferroelectric. *Science* **2006**, *313*, 181−183.

(2) Zhuravlev, M. Y.; Sabirianov, R. F.; Jaswal, S.; Tsymbal, E. Y. Giant electroresistance in ferroelectric tunnel junctions. *Phys. Rev. Lett.* **2005**, *94*, 246802.

(3) Kohlstedt, H.; Pertsev, N.; Contreras, J. R.; Waser, R. Theoretical current-voltage characteristics of ferroelectric tunnel junctions. *Phys. Rev. B: Condens. Matter Mater. Phys.* **2005**, *72*, 125341.

(4) Chanthbouala, A.; Crassous, A.; Garcia, V.; Bouzehouane, K.; Fusil, S.; Moya, X.; Allibe, J.; Dlubak, B.; Grollier, J.; Xavier, S.; et al. Solid-state memories based on ferroelectric tunnel junctions. *Nat. Nanotechnol.* **2012**, *7*, 101.

(5) Kim, D. J.; Lu, H.; Ryu, S.; Bark, C.-W.; Eom, C.-B.; Tsymbal, E. Y.; Gruverman, A. Ferroelectric tunnel memristor. *Nano Lett.* **2012**, *12*, 5697−5702.

(6) Garcia, V.; Bibes, M. Ferroelectric tunnel junctions for information storage and processing. *Nat. Commun.* **2014**, *5*, 4289.

(7) Velev, J. P.; Burton, J. D.; Zhuravlev, M. Y.; Tsymbal, E. Y. Predictive modelling of ferroelectric tunnel junctions. *npj Computational Materials* **2016**, *2*, 16009.

DOI: 10.1021/acs.nanolett.9b03056
Nano Lett. 2019, 19, 7385−7393

(8) Zenkevich, A.; Minnekaev, M.; Matveyev, Y.; Lebedinskii, Y.; Bulakh, K.; Chouprik, A.; Baturin, A.; Maksimova, K.; Thiess, S.; Drube, W. Electronic band alignment and electron transport in Cr/$BaTiO_3$/Pt ferroelectric tunnel junctions. *Appl. Phys. Lett.* **2013**, *102*, 062907.
(9) Soni, R.; Petraru, A.; Meuffels, P.; Vavra, O.; Ziegler, M.; Kim, S. K.; Jeong, D. S.; Pertsev, N. A.; Kohlstedt, H. Giant electrode effect on tunnelling electroresistance in ferroelectric tunnel junctions. *Nat. Commun.* **2014**, *5*, 5414.
(10) Tao, L. L.; Wang, J. Ferroelectricity and tunneling electroresistance effect in asymmetric ferroelectric tunnel junctions. *J. Appl. Phys.* **2016**, *119*, 224104.
(11) Tsurumaki-Fukuchi, A.; Yamada, H.; Sawa, A. Resistive switching artificially induced in a dielectric/ferroelectric composite diode. *Appl. Phys. Lett.* **2013**, *103*, 152903.
(12) Lu, H.; Lipatov, A.; Ryu, S.; Kim, D. J.; Lee, H.; Zhuravlev, M. Y.; Eom, C.-B.; Tsymbal, E. Y.; Sinitskii, A.; Gruverman, A. Ferroelectric tunnel junctions with graphene electrodes. *Nat. Commun.* **2014**, *5*, 5518.
(13) Borisov, V. S.; Ostanin, S.; Achilles, S.; Henk, J.; Mertig, I. Spin-dependent transport in a multiferroic tunnel junction: Theory for Co/$PbTiO_3$/Co. *Phys. Rev. B: Condens. Matter Mater. Phys.* **2015**, *92*, 075137.
(14) Tao, L. L.; Wang, J. Ferroelectricity and tunneling electroresistance effect driven by asymmetric polar interfaces in all-oxide ferroelectric tunnel junctions. *Appl. Phys. Lett.* **2016**, *108*, 062903.
(15) Jiang, L.; Tao, L. L.; Yang, B. S.; Wang, J.; Han, X. F. Enhanced tunneling electroresistance in multiferroic tunnel junctions due to the reversible modulation of orbitals overlap. *Appl. Phys. Lett.* **2016**, *109*, 192902.
(16) Bilc, D. I.; Novaes, F. D.; Íñiguez, J.; Ordejón, P.; Ghosez, P. Electroresistance effect in ferroelectric tunnel junctions with symmetric electrodes. *ACS Nano* **2012**, *6*, 1473−1478.
(17) Useinov, A.; Kalitsov, A.; Velev, J.; Kioussis, N. Bias-dependence of the tunneling electroresistance and magnetoresistance in multiferroic tunnel junctions. *Appl. Phys. Lett.* **2014**, *105*, 102403.
(18) Lu, H.; Lee, D.; Klyukin, K.; Tao, L.; Wang, B.; Lee, H.; Lee, J.; Paudel, T. R.; Chen, L.-Q.; Tsymbal, E. Y.; et al. Tunneling hot spots in ferroelectric $SrTiO_3$. *Nano Lett.* **2018**, *18*, 491−497.
(19) Klyukin, K.; Tao, L. L.; Tsymbal, E. Y.; Alexandrov, V. Defect-assisted tunneling electroresistance in ferroelectric tunnel junctions. *Phys. Rev. Lett.* **2018**, *121*, 056601.
(20) Pantel, D.; Goetze, S.; Hesse, D.; Alexe, M. Room-temperature ferroelectric resistive switching in ultrathin $Pb(Zr_{0.2}Ti_{0.8})O_3$ films. *ACS Nano* **2011**, *5*, 6032−6038.
(21) Pantel, D.; Lu, H.; Goetze, S.; Werner, P.; Kim, D. J.; Gruverman, A.; Hesse, D.; Alexe, M. Tunnel electroresistance in junctions with ultrathin ferroelectric $Pb(Zr_{0.2}Ti_{0.8})O_3$ barriers. *Appl. Phys. Lett.* **2012**, *100*, 232902.
(22) Radaelli, G.; Gutiérrez, D.; Sánchez, F.; Bertacco, R.; Stengel, M.; Fontcuberta, J. Large room-temperature electroresistance in dual-modulated ferroelectric tunnel barriers. *Adv. Mater.* **2015**, *27*, 2602−2607.
(23) Wen, Z.; Li, C.; Wu, D.; Li, A.; Ming, N. Ferroelectric-field-effect-enhanced electroresistance in metal/ferroelectric/semiconductor tunnel junctions. *Nat. Mater.* **2013**, *12*, 617.
(24) Tsymbal, E. Y.; Gruverman, A. Ferroelectric tunnel junctions: beyond the barrier. *Nat. Mater.* **2013**, *12*, 602.
(25) Li, C.; Huang, L.; Li, T.; Lü, W.; Qiu, X.; Huang, Z.; Liu, Z.; Zeng, S.; Guo, R.; Zhao, Y.; et al. Ultrathin $BaTiO_3$-based ferroelectric tunnel junctions through interface engineering. *Nano Lett.* **2015**, *15*, 2568−2573.
(26) Liu, X.; Burton, J. D.; Tsymbal, E. Y. Enhanced tunneling electroresistance in ferroelectric tunnel junctions due to the reversible metallization of the barrier. *Phys. Rev. Lett.* **2016**, *116*, 197602.
(27) Wang, X.; Song, B.; Tao, L. L.; Wen, J.; Zhang, L.; Zhang, Y.; Lv, Z.; Tang, J.; Sui, Y.; Song, B.; et al. Effect of a semiconductor electrode on the tunneling electroresistance in ferroelectric tunneling junction. *Appl. Phys. Lett.* **2016**, *109*, 163501.
(28) Li, T.; Sharma, P.; Lipatov, A.; Lee, H.; Lee, J.-W.; Zhuravlev, M. Y.; Paudel, T. R.; Genenko, Y. A.; Eom, C.-B.; Tsymbal, E. Y.; et al. Polarization-mediated modulation of electronic and transport properties of hybrid MoS_2−$BaTiO_3$−$SrRuO_3$ tunnel junctions. *Nano Lett.* **2017**, *17*, 922−927.
(29) Xi, Z.; Ruan, J.; Li, C.; Zheng, C.; Wen, Z.; Dai, J.; Li, A.; Wu, D. Giant tunnelling electroresistance in metal/ferroelectric/semiconductor tunnel junctions by engineering the Schottky barrier. *Nat. Commun.* **2017**, *8*, 15217.
(30) Zhuravlev, M. Y.; Wang, Y.; Maekawa, S.; Tsymbal, E. Y. Tunneling electroresistance in ferroelectric tunnel junctions with a composite barrier. *Appl. Phys. Lett.* **2009**, *95*, 052902.
(31) Caffrey, N. M.; Archer, T.; Rungger, I.; Sanvito, S. Coexistance of giant tunneling electroresistance and magnetoresistance in an all-oxide composite magnetic tunnel junction. *Phys. Rev. Lett.* **2012**, *109*, 226803.
(32) Wu, Q.; Shen, L.; Yang, M.; Zhou, J.; Chen, J.; Feng, Y. P. Giant tunneling electroresistance induced by ferroelectrically switchable two-dimensional electron gas at nonpolar $BaTiO_3$/$SrTiO_3$ interface. *Phys. Rev. B: Condens. Matter Mater. Phys.* **2016**, *94*, 155420.
(33) Fredrickson, K. D.; Demkov, A. A. Switchable conductivity at the ferroelectric interface: nonpolar oxides. *Phys. Rev. B: Condens. Matter Mater. Phys.* **2015**, *91*, 115126.
(34) Aguado-Puente, P.; Bristowe, N. C.; Yin, B.; Shirasawa, R.; Ghosez, P.; Littlewood, P. B.; Artacho, E. Model of two-dimensional electron gas formation at ferroelectric interfaces. *Phys. Rev. B: Condens. Matter Mater. Phys.* **2015**, *92*, 035438.
(35) Wang, L.; Cho, M. R.; Shin, Y. J.; Kim, J. R.; Das, S.; Yoon, J.-G.; Chung, J.-S.; Noh, T. W. Overcoming the fundamental barrier thickness limits of ferroelectric tunnel junctions through $BaTiO_3$/$SrTiO_3$ composite barriers. *Nano Lett.* **2016**, *16*, 3911−3918.
(36) Ohtomo, A.; Muller, D. A.; Grazul, J. L.; Hwang, H. Y. Artificial charge-modulationin atomic-scale perovskite titanate superlattices. *Nature* **2002**, *419*, 378−380.
(37) Ohtomo, A.; Hwang, H. Y. A high-mobility electron gas at the $LaAlO_3$/$SrTiO_3$ heterointerface. *Nature* **2004**, *427*, 423−426.
(38) Nakagawa, N.; Hwang, H. Y.; Muller, D. A. Why some interfaces cannot be sharp. *Nat. Mater.* **2006**, *5*, 204−209.
(39) Lee, H.; Campbell, N.; Lee, J.; Asel, T. J.; Paudel, T. R.; Zhou, H.; Lee, J. W.; Noesges, B.; Seo, J.; Park , B.; Brillson, L. J.; Oh, S. H.; Tsymbal, E. Y.; Rzchowski, M. S.; Eom, C. B. Direct observation of a two-dimensional hole gas at oxide interfaces. *Nat. Mater.* **2018**, *17*, 231−236.
(40) Thiel, S.; Hammerl, G.; Schmehl, A.; Schneider, C.; Mannhart, J. Tunable quasi-two-dimensional electron gases in oxide heterostructures. *Science* **2006**, *313*, 1942−1945.
(41) Bark, C. W.; Felker, D. A.; Wang, Y.; Zhang, Y.; Jang, H. W.; Folkman, C. M.; Park, J. W.; Baek, S. H.; Zhou, H.; Fong, D. D.; Pan, X. Q.; Tsymbal, E. Y.; Rzchowski, M. S.; Eom, C. B. Tailoring a two-dimensional electron gas at the $LaAlO_3$/$SrTiO_3$ (001) interface by epitaxial strain. *Proc. Natl. Acad. Sci. U. S. A.* **2011**, *108*, 4720−4724.
(42) Sharma, P.; Ryu, S.; Burton, J. D.; Paudel, T. R.; Bark, C. W.; Huang, Z.; Tsymbal, E. Y.; Catalan, G.; Eom, C. B.; Gruverman, A. Mechanical tuning of $LaAlO_3$/$SrTiO_3$ interface conductivity. *Nano Lett.* **2015**, *15*, 3547−3551.
(43) Zhang, F.; Lv, P.; Zhang, Y.; Huang, S.; Wong, C.-M.; Yau, H.-M.; Chen, X.; Wen, Z.; Jiang, X.; Zeng, C.; Hong, J.; Dai, J.-Y. Modulating the electrical transport in the two-dimensional electron gas at $LaAlO_3$/$SrTiO_3$ heterostructures by interfacial flexoelectricity. *Phys. Rev. Lett.* **2019**, *122*, 257601.
(44) Wang, S.; Bai, Y.; Xie, L.; Li, C.; Key, J. D.; Wu, D.; Wang, P.; Pan, X. Ferroelectric polarization-modulated interfacial fine structures involving two-dimensional electron gases in Pb(Zr,Ti)O_3/$LaAlO_3$/$SrTiO_3$ heterostructures. *ACS Appl. Mater. Interfaces* **2018**, *10*, 1374−1382.
(45) Gao, Z.; Huang, X.; Li, P.; Wang, L.; Wei, L.; Zhang, W.; Guo, H. Reversible resistance switching of 2D electron gas at $LaAlO_3$/$SrTiO_3$ heterointerface. *Adv. Mater. Interfaces* **2018**, *5*, 1701565.

DOI: 10.1021/acs.nanolett.9b03056
Nano Lett. 2019, 19, 7385−7393

(46) Kim, S.-I.; Kim, D.-H.; Kim, Y.; Moon, S. Y.; Kang, M.-G.; Choi, J. K.; Jang, H. W.; Kim, S. K.; Choi, J.-W.; Yoon, S.-J.; Chang, H. J.; Kang, C.-Y.; Lee, S.; Hong, S.-H.; Kim, J.-S.; Baek, S.-H. Nonvolatile control of 2DEG conductivity at oxide interfaces. *Adv. Mater.* **2013**, *25*, 4612−4617.
(47) Kim, S.-I.; Gwon, H. J.; Kim, D.-H.; Kim, S. K.; Choi, J.-W.; Yoon, S.-J.; Chang, H. J.; Kang, C.-Y.; Kwon, B.; Bark, C.-W. Giant electroresistive ferroelectric diode on 2DEG. *Sci. Rep.* **2015**, *5*, 10548.
(48) Niranjan, M. K.; Wang, Y.; Jaswal, S. S.; Tsymbal, E. Y. Prediction of a switchable two-dimensional electron gas at ferroelectric oxide interfaces. *Phys. Rev. Lett.* **2009**, *103*, 016804.
(49) Tra, V. T.; Chen, J.-W.; Huang, P.-C.; Huang, B.-C.; Cao, Y.; Yeh, C.-H.; Liu, H.-J.; Eliseev, E. A.; Morozovska, A. N.; Lin, J.-Y.; et al. Ferroelectric control of the conduction at the $LaAlO_3/SrTiO_3$ heterointerface. *Adv. Mater.* **2013**, *25*, 3357−3364.
(50) Medarde, M. L. Structural, magnetic and electronic properties of $RNiO_3$ perovskites (R= rare earth). *J. Phys.: Condens. Matter* **1997**, *9*, 1679.
(51) Gou, G.; Grinberg, I.; Rappe, A. M.; Rondinelli, J. M. Lattice normal modes and electronic properties of the correlated metal $LaNiO_3$. *Phys. Rev. B: Condens. Matter Mater. Phys.* **2011**, *84*, 144101.
(52) Tao, L. L.; Tsymbal, E. Y. Two-dimensional type-II Dirac fermions in a $LaAlO_3/LaNiO_3/LaAlO_3$ quantum well. *Phys. Rev. B: Condens. Matter Mater. Phys.* **2018**, *98*, 121102.
(53) Peng, J. J.; Song, C.; Cui, B.; Li, F.; Mao, H. J.; Wang, G. Y.; Pan, F. Manipulation of orbital occupancy by ferroelectric polarization in $LaNiO_3/BaTiO_{3-\delta}$ heterostructures. *Appl. Phys. Lett.* **2015**, *107*, 182904.
(54) Kresse, G.; Joubert, D. From ultrasoft pseudopotentials to the projector augmented-wave method. *Phys. Rev. B: Condens. Matter Mater. Phys.* **1999**, *59* (3), 1758.
(55) Han, M.-G.; Marshall, M. S.; Wu, L.; Schofield, M. A.; Aoki, T.; Twesten, R.; Hoffman, J.; Walker, F. J.; Ahn, C. H.; Zhu, Y. Interface-induced nonswitchable domains in ferroelectric thin films. *Nat. Commun.* **2014**, *5*, 4693.
(56) Li, M.; Tao, L. L.; Velev, J. P.; Tsymbal, E. Y. Resonant tunneling across a ferroelectric domain wall. *Phys. Rev. B: Condens. Matter Mater. Phys.* **2018**, *97*, 155121.
(57) Smogunov, A.; Dal Corso, A.; Tosatti, E. Ballistic conductance of magnetic Co and Ni nanowires with ultrasoft pseudopotentials. *Phys. Rev. B: Condens. Matter Mater. Phys.* **2004**, *70*, 045417.
(58) Giannozzi, P.; Baroni, S.; Bonini, N.; Calandra, M.; Car, R.; Cavazzoni, C.; Ceresoli, D.; Chiarotti, G. L.; Cococcioni, M.; Dabo, I.; et al. QUANTUM ESPRESSO: a modular and open-source software project for quantum simulations of materials. *J. Phys.: Condens. Matter* **2009**, *21* (39), 395502.
(59) Sanchez-Santolino, G.; Tornos, J.; Hernandez-Martin, D.; Beltran, J. I.; Munuera, C.; Cabero, M.; Perez-Muñoz, A.; Ricote, J.; Mompean, F.; Garcia-Hernandez, M.; et al. Resonant electron tunnelling assisted by charged domain walls in multiferroic tunnel junctions. *Nat. Nanotechnol.* **2017**, *12*, 655.
(60) Tsymbal, E. Y.; Velev, J. P. Ferroelectric tunnel junctions: Crossing the wall. *Nat. Nanotechnol.* **2017**, *12*, 614.

DOI: 10.1021/acs.nanolett.9b03056
Nano Lett. 2019, 19, 7385−7393